iScience

CellPress
OPEN ACCESS

Perspective

Fresh water production from atmospheric air: Technology and innovation outlook

Robin Peeters,[1] Hannah Vanderschaeghe,[1] Jan Rongé,[1] and Johan A. Martens[1,*]

SUMMARY

Capturing water vapor from atmospheric air is a possible solution to local water scarcity, but it is very energy demanding. Energy consumption estimates of water-from-air technologies involving adsorption processes, thermo-responsive hydrophilicity switching polymers, air cooling processes, and reverse osmosis of deliquescent salt solutions reveal that these technologies are not competitive when compared with seawater desalination, and the use of fresh water and wastewater sources. They only become a viable option in the absence of local liquid water sources and when long-distance transport for socio-economic reasons is not an option. Of interest, direct solar-driven technology for water-from-air production is an attractive means to disentangle the local water-energy nexus. It is expected that climate change will accelerate the introduction of water-from-air technologies in local water supply schemes. The optimal water-from-air technology depends on the climate, relative humidity, and temperature profiles. A world map is presented, indicating the optimal geographic location for each technology.

INTRODUCTION

Water can be considered one of the most valuable commodities on Earth. This becomes apparent by the plethora of human activities competing for this scarce resource. The domestic sector requires water for household chores and drinking purposes, industry uses water as solvent or chemical feedstock, thermoelectric power plants need water as a coolant, and irrigation water is essential for agriculture, which is responsible for most of the water demand (IEA, 2016; Mekonnen and Hoekstra, 2011; Chapagain and Hoekstra, 2004). The large variety of water uses makes local water scarcity a severe problem. Several billion people are expected to live in water-stressed areas in the near future (IEA, 2016; Urban, 2017). A growing world population combined with deteriorating water quality, falling groundwater levels, and the intensification of the water-energy nexus make the water scarcity problem ever more prominent (IEA, 2016). Water on Earth is abundant; however, most of this water is not directly useful either because it is saline, present in deep aquifers and difficult to reach, or present in the solid state as snow or ice or vapor in the atmosphere (Shiklomanov, 1993). Water scarcity is largely a regional or seasonal phenomenon caused by the dynamic hydrological cycle. Increasing the local production of water is a logical solution to the water scarcity problem.

Water vapor present in the air is a water resource that is available everywhere on the planet and is currently hardly exploited. Regions affected by drought and adverse climate change may consider capturing water vapor from the air for fresh water production (Gad et al., 2001; Tu et al., 2018; Peeters et al., 2020; Akbar Salehi et al., 2020; Jarimi et al., 2020; Raveesh et al., 2021). Dew harvesting, fog collection, active air cooling, and desiccant-based water harvesting are the main water harvesting technologies. Especially the development of superior desiccants for designing such decentralized water vapor capturing systems is receiving lots of interest in the academic world (Tu et al., 2018; Peeters et al., 2020; Akbar Salehi et al., 2020; Jarimi et al., 2020; Raveesh et al., 2021). Efficient desiccants have been proposed, like metal-organic framework MIL-101 with LiCl, MOF-801, MOF-303, and alginate gel with $CaCl_2$ (Xu et al., 2020; Kallenberger and Fröba, 2018; Kim et al., 2017; Hanikel et al., 2019). Some desiccants have a large water vapor adsorption capacity even at very low relative humidity and high ambient temperatures typical of arid regions (Xu et al., 2020; Kallenberger and Fröba, 2018; Kim et al., 2017; Hanikel et al., 2019; Elashmawy, 2020). The recovery of water from such desiccants is achieved by heating, causing evaporative desorption. To obtain liquid water, water vapor desorbing from desiccants needs to be condensed again by cooling (Figure 1). The high energy demand incurred by these process steps is the main obstacle to the widespread application of current

[1]Centre for Surface Chemistry and Catalysis, KU Leuven, Celestijnenlaan 200f – bus 2461, Leuven 3001, Belgium

*Correspondence: johan.martens@kuleuven.be

https://doi.org/10.1016/j.isci.2021.103266

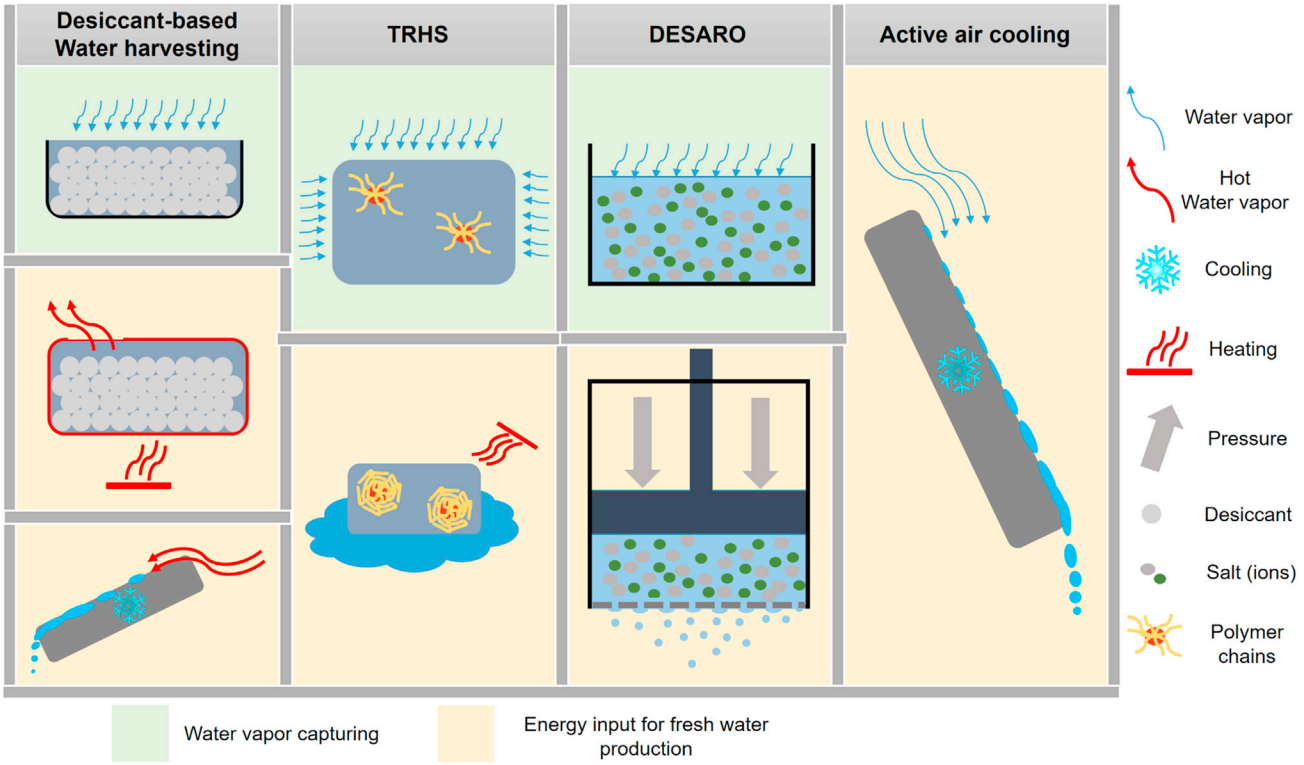

Figure 1. The four main atmospheric water harvesting processes
Each individual process is covered in more detail throughout the text.

water-from-air production methods. Energy consumption is estimated to be responsible for 50% of the total cost of commercial water-from-air harvesting devices (Peeters et al., 2020; Akbar Salehi et al., 2020). Using electricity generated in thermoelectric power plants with water as coolant aggravates the water-energy nexus. The specific water yield (L/kWh) of water-from-air technologies may be even less than the water consumed in the electricity generation process (Urban, 2017; Peeters et al., 2020; Lee et al., 2016).

Alternative concepts for atmospheric water harvesting avoiding energy-intensive phase transitions have been less investigated. Thermo-responsive hydrophilicity switching (TRHS) polymers have an attractive feature in this respect. These materials change configuration upon heating and become hydrophobic such that absorbed water is expulsed directly in liquid form (Figure 1) (Zhao et al., 2019; Matsumoto et al., 2018; Coronado et al., 2011; Afroze et al., 2000; Takigawa et al., 2001; Karmakar et al., 2020). Another concept that is energetically attractive that we propose is to produce a salt solution by wetting a deliquescent salt with water vapor from atmospheric air and to apply reverse osmosis (DESARO), on analogy with seawater desalination (Figure 1). Both concepts will be compared with desiccant-based water harvesting and the basic concept of directly cooling the air below the dew point in an active air cooling device (Figure 1). The list of fresh water production technologies currently being handled in water-energy nexus analyses (IEA, 2016) is expanded with these technologies. Estimation of climate-dependent specific water yields (liters of water produced per kWh) derived from energy balances according to different water vapor capturing principles are provided in this work. A geographic map indicating the optimal water-from-air technology is included.

WATER-FROM-AIR TECHNOLOGIES INVOLVING THREE WATER PHASE TRANSITIONS

Desiccants can be used to capture air moisture even at low relative humidity (Kim et al., 2017). Desiccants function via adsorption of water vapor on a hydrophilic porous adsorbent, absorption in a hygroscopic medium, or a combination of both (Xu et al., 2020; Kim et al., 2018). There is significant progress in desiccant materials development for capturing water vapor, and remarkably high adsorption capacities at low relative humidity have been reported (Tu et al., 2018; Peeters et al., 2020; Akbar Salehi et al., 2020; Jarimi et al.,

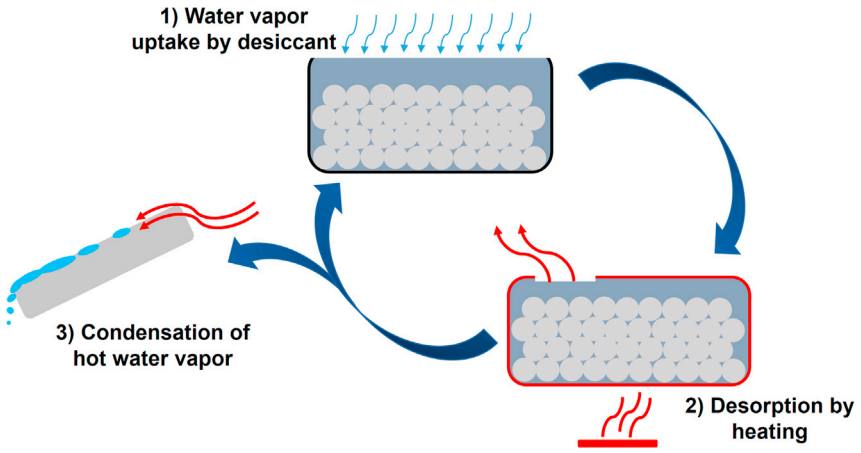

Figure 2. The desiccant-based water harvesting process

Water phase transitions of the desiccant-based water harvesting process: (1) water vapor ad- or absorption on a desiccant material; (2) evaporative desorption upon heating of desiccant material; (3) condensation by cooling of hot water-saturated air (Kim et al., 2017; Alayli et al., 1987).

2020; Raveesh et al., 2021; Xu et al., 2020; Kallenberger and Fröba, 2018; Kim et al., 2017; Hanikel et al., 2019; Li et al., 2018; Sleiti et al., 2021; Asim et al., 2021; Entezari et al., 2020; Ejeian et al., 2020; Wang et al., 2021). Recovery of the captured water is achieved by thermal evacuation of the water in vapor state from the desiccant material. The passive desiccant approach using direct solar heating is most common. The obtained hot water vapor subsequently needs cooling to cause condensation to obtain liquid water (Tu et al., 2018; Peeters et al., 2020; Akbar Salehi et al., 2020; Jarimi et al., 2020). Overall, three water phase transitions are involved in such processes with ad- and absorbents: (1) from airborne vapor to ad- or absorbed state, (2) from ad- or absorbed state to vapor, and (3) from vapor to liquid (Figure 2).

The energy requirements of the desiccant-based water harvesting process are conveniently expressed as the maximum specific water yield (L/kWh) (Peeters et al., 2020). The ad(ab)sorption step is exothermic and does not need any energy input unless convection is insufficient to move air to the desiccant using active ventilation. In the estimation of energy needs, ventilation is neglected. The maximum specific water yield of desiccant-based water harvesting $SY_{max,\ DES}$ is limited by three energy needs (Equation 1).

$$SY_{max,\ DES} = \frac{3,600,000}{\Delta H^{des} + C_{p,w}(T_{des} - T_{amb}) + \Delta H^{cond}} \quad \text{(Equation 1)}$$

Energy is required to heat the saturated desiccant and to provide the desorption heat to evacuate the captured water from the desiccant material as a hot vapor. In a subsequent step, heat has to be dissipated in order to condense the hot water vapor and to collect liquid water. The parameter values used in the specific water yield estimation are given in Table 1. The latent heat parameters ΔH^{des} and ΔH^{cond} represent the heat of desorption and condensation heat dissipation, respectively. The sensible heat contribution is obtained from the liquid water heat capacity $C_{p,w}$ and the difference between the desorption temperature T_{des} and the initial desiccant temperature at ambient conditions T_{amb}. The desiccant heat capacity, especially for porous materials, is significantly lower than the heat capacity of water and is, therefore, neglected (Chakraborty et al., 2009; Incropera et al., 2013). The parameters ΔH^{des} and T_{des} are ad(ab)sorbent-dependent properties (Kim et al., 2016; Fathieh et al., 2018).

The ambient temperature T_{amb} selected in the range 5°C–35°C defining sensible heat requirements appears to entail little differences in the total energy demand of this water harvesting process. Depending on the desorption heat, the maximum specific water yield is estimated to be 0.34–0.73 L/kWh, calculated over a wide range of water desorption enthalpies (Table 1). Neglecting condensation heat evacuation increases the specific water yield to 0.43–1.34 L/kWh.

Experimental specific water yields of 0.12–0.75 L/kWh (neglecting condensation heat) have been reported in the literature for desiccant-based water harvesting under different climate conditions. The lower range of

Table 1. Parameter values used for estimating the maximum specific water yield of desiccant-based technology

Parameter	Value	Reference
ΔH^{des}	2,500,000–8,000,000 J/kg	(Kim et al., 2016)
ΔH^{cond}	2,257,000 J/kg (@100°C)	(Incropera et al., 2013)
T_{des}	80°C	(Peeters et al., 2020)
T_{amb}	5°C–35°C	
$C_{p,w}$	4,185 J/kg.K	(Incropera et al., 2013)

values is attributed to low thermal efficiencies, usually between 30% and 40% (Peeters et al., 2020; Xu et al., 2020; Elashmawy, 2020; Kim et al., 2018; Li et al., 2018, 2020). Implementation of photothermal materials or materials with high thermal conductivity has led to considerable solar-to-thermal efficiency gains of up to 70% during water desorption (Peeters et al., 2020; Li et al., 2018, 2020; Mulchandani et al., 2020). A specific water yield of 0.84 L/kWh was achieved by using an efficient heater in an active desiccant-based water harvesting cycle working more efficiently than solar heating (Wang et al., 2017). In addition, improvements in device design to reduce heat losses, adoption of latent heat recovery measures, and thermally insulating the condensation surfaces are beneficial for improving the overall efficiency (Tu et al., 2018; Peeters et al., 2020; Raveesh et al., 2021; Li et al., 2018, 2020; LaPotin et al., 2021; Hua et al., 2021). The desiccant choice and system configuration play a key role in achieving high water output at high energy efficiency and low cost. Next to adsorption capacity and the shape of the water adsorption isotherm, water adsorption kinetics are crucial to perform multiple sorption-desorption cycles per day to enhance the water production rate (Fathieh et al., 2018; LaPotin et al., 2019, 2021; Zhou et al., 2020a).

WATER-FROM-AIR TECHNOLOGIES INVOLVING A SINGLE WATER PHASE TRANSITION

Thermo-responsive hydrophilicity switching

TRHS polymers are a class of materials that capture water via a combination of ad- and absorption. Remarkable is that the captured water vapor can be recovered directly in a liquid state instead of vapor. Heating a saturated TRHS material to the hydrophilicity switching temperature makes the material hydrophobic and water repellent, and this causes the captured water to leak out (Figure 3) (Zhao et al., 2019).

In the estimation of the maximum specific water yield for thermo-responsive materials $SY_{max,TRHS}$, two energy contributions need to be considered (Equation 2). Heating is needed to increase the temperature to the hydrophilicity switching point (T_{HS}), and additional energy is required to enable the configurational change of the polymer ΔH^{HS}. In the estimation of the maximum specific water yield, a linear sorption

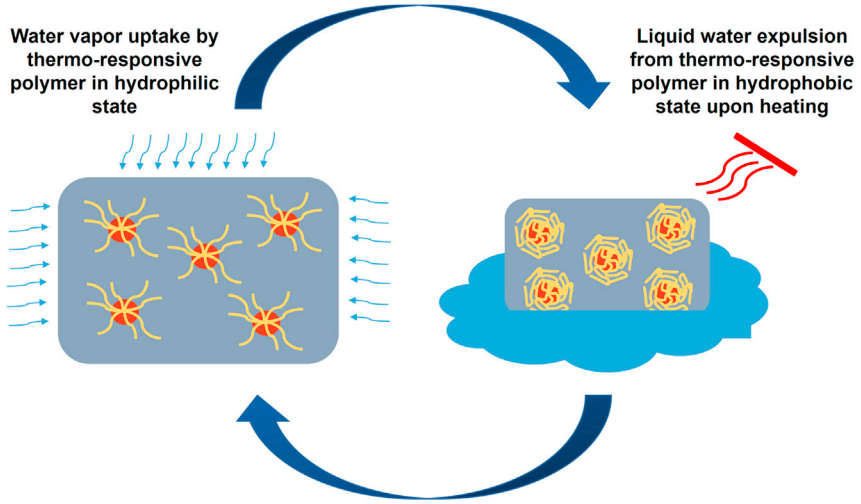

Figure 3. Water harvesting cycle of a thermo-responsive material

Thermo-responsive hydrophilicity switching material ad(ab)sorbs water vapor at low temperature and releases liquid water by hydrophilicity switching upon heating (Zhao et al., 2019).

Table 2. Parameter values used for estimating the maximum specific water yield of thermo-responsive hydrophilicity switching polymers

Parameter	Value	Reference
ΔH^{HS}	3,000 J/kg	(Coronado et al., 2011)
T_{HS}	40°C	(Zhao et al., 2019)
τ	7	(Zhao et al., 2019)
δ	0.4	(Zhao et al., 2019)

isotherm was assumed ($\tau\Phi$) for simplification with constant τ and relative humidity Φ. Parameter values are provided in Table 2. The temperature for hydrophilicity switching $T_{HS}$is considered to be 40°C (Zhao et al., 2019). A fraction of the captured water is left behind and cannot be removed by the TRHS process, reducing the overall efficiency of the water expulsion process. The remaining water corresponds to the water capacity at relative humidity δ.

$$SY_{max,TRHS} = \frac{3,600,000}{\frac{\Delta H^{HS}}{\tau\Phi} + C_{p,w}(T_{HS} - T_{amb})}\left(\frac{\Phi - \delta}{\Phi}\right) \quad \text{(Equation 2)}$$

The maximum specific water yield is plotted in Figure 4 for a realistic case ($\delta = 0.4$) where the water below the 40% relative humidity mark on the isotherm cannot be removed by the TRHS process. The main energy input is the sensible heat needed to increase the temperature of the saturated TRHS material to the hydrophilicity switching point. The ambient temperature is, therefore, the dominant parameter governing performance. Sensible heat requirements are small for ambient temperatures close to the hydrophilicity switching temperature. The phase change of poly(N-isopropylacrylamide) amounts to 3,000 J/kg (Coronado et al., 2011). This term represents only a minor contribution to the maximum specific water yield and becomes slightly more important only at low relative humidity with T_{amb} close to T_{HS}, such as, e.g., 35°C. The theoretical maximum specific water yield of the TRHS process varies considerably with relative humidity. This is due to the diminishing water recovery potential close to the humidity threshold δ.

The specific water yields practically achieved by this relatively new method are 9.28 and 3.71 L/kWh at 90% and 60% relative humidity, respectively (Peeters et al., 2020; Zhao et al., 2019). These values are small compared with the possible maxima in the range of typical ambient temperatures of 15°C–25°C (Figure 4). Water yields of 20–30 L/kWh and 10–20 L/kWh are achievable at 90% and 60% relative humidity, respectively. The low experimentally achieved efficiencies are attributed to excessive heat losses to the environment by heating the material in the open air and to the occurrence of water evaporation in parallel to liquid water expulsion. A simple experimental design comes at the cost of reduced energy efficiencies.

Deliquescent salt reverse osmosis

A new concept proposed here for avoiding energy-intensive water phase transitions in water-from-air capturing processes is deliquescent salt reverse osmosis (DESARO). It makes use of the strong affinity of salts for water vapor absorption and the reverse osmosis separation principle known from seawater desalination. Salts such as LiCl are hygroscopic and above a critical water content they become a concentrated salt solution. This happens at the deliquescent relative humidity (Mauer and Taylor, 2010; Tereshchenko, 2015). Increasing the relative humidity above this level results in additional water absorption, which dilutes the salt solution (Figure 5). The absorption process continues until the water activity of the solution equals that of water vapor at that relative humidity (Mauer and Taylor, 2010; Tereshchenko, 2015; Linnow et al., 2014; Cantrell et al., 2002; Davila et al., 2010).

Instead of evaporating water from the salt solution and condensing it, in analogy with the desiccant-based technology, in DESARO liquid water is recovered using the pressure-driven reverse osmosis (RO) technique (Figure 6). The retentate of the separation step is reused in the next cycle to absorb water from the air again. A major cost and environmental concern of commercial seawater desalination plants is the disposal of the retentate (Davenport et al., 2018; Rautenbach and Linn, 1996). This aspect is absent in the DESARO process because the retentate is reused cyclically.

Estimation of the intrinsic energy requirement of DESARO is based on the minimum pressure that has to be exerted to overcome the osmotic pressure to separate water from the salt solution. The osmotic pressure is

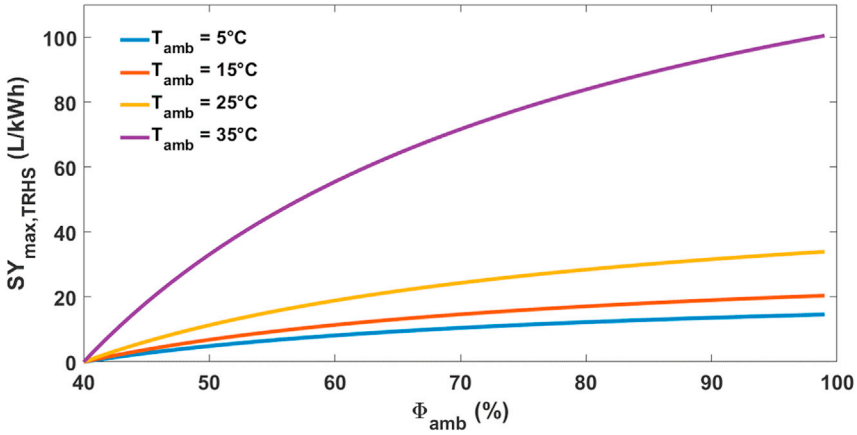

Figure 4. Maximum specific water yield of TRHS technology ($SY_{max,\ TRHS}$) against relative humidity at different ambient air temperatures

Parameters values of Table 2 are used.

estimated from the liquid-vapor equilibrium of a non-ideal ionic salt solution (Equation 3) in which γ_w is the activity coefficient of liquid water, x_w the mole fraction of water in the liquid phase, y_w the water mole fraction in the gas phase, P the total air pressure, P_s the water vapor saturation pressure, and P_w the water vapor pressure (Sandler, 2006).

$$x_w \gamma_w P_s(T) = y_w P = P_w \quad \text{(Equation 3)}$$

The term $x_w \gamma_w$ equals the relative humidity Φ (Equation 4).

$$x_w \gamma_w = \frac{P_w}{P_s(T)} = \Phi \quad \text{(Equation 4)}$$

The osmotic pressure π_0 (Pa) is given in Equation 5 with $\underline{V}_w^L$, the molar volume of water ($18*10^{-6}$ m^3/mol) (Sandler, 2006).

$$\pi_0 = \frac{-RT}{\underline{V}_w^L} ln(x_w \gamma_w) \quad \text{(Equation 5)}$$

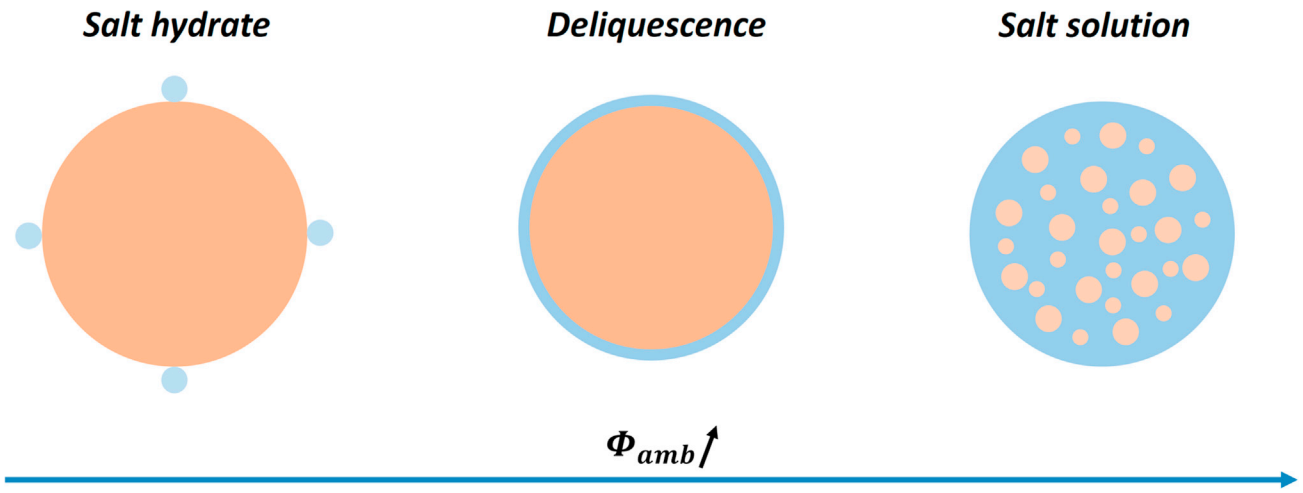

Figure 5. The deliquescence process

Stages of water uptake from the air by hygroscopic salt. Water is adsorbed on the surface of solid salt crystals below the deliquescence relative humidity. Above this humidity level, the salt starts to dissolve and a saturated solution is formed. Increasing the relative humidity causes dilution of the salt solution (Mauer and Taylor, 2010).

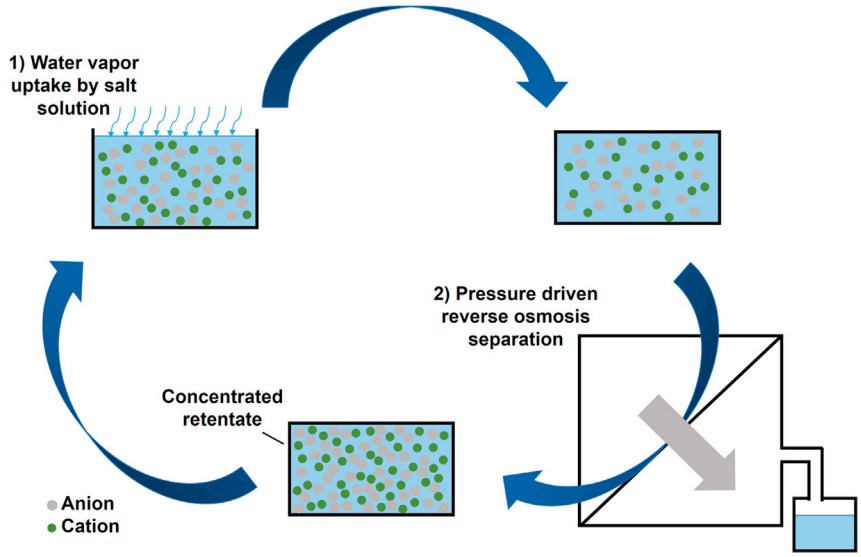

Figure 6. Deliquescent salt desalination by the reverse osmosis process

A salt solution absorbs water from the air and becomes more diluted (1). Fresh water is produced by pressure-driven reverse osmosis (2) and concentrated salt retentate is reused for water capture.

From the liquid-vapor equilibrium (Equation 4) it follows that the osmotic pressure is a logarithmic function of relative humidity (Equation 6) and this pressure is independent of the nature of the salt.

$$\pi_0 = \frac{-RT}{V_w^L} ln(\Phi) \quad \text{(Equation 6)}$$

The pressure π_0 denotes the minimum pressure that must be exerted on the salt solution to prevent water transport from the fresh water to the saline waterside. To account for water production, this pressure is related to the osmotic pressure π_Y (Equation 7) by taking into account the permeate water recovery Y, defined as the ratio of the permeate to the feed flow. It pertains to high salt rejection processes. The retentate pressure at the exit should at least equal the minimum osmotic pressure π_Y at the desired recovery value (Zhu et al., 2009). In real applications, an overpressure must be applied to achieve a desired water flux through the membrane and to counteract concentration polarization effects and fouling resistance (Zhu et al., 2009; Shrivastava and Stevens, 2018).

$$\pi_Y = \frac{\pi_0}{1-Y} \quad \text{(Equation 7)}$$

Figure 7 shows the evolution of the osmotic pressure π_Y as a function of water recovery for salt mixtures at different initial equilibria. A typical RO process is executed in a single-stage configuration operating at a fixed outlet pressure (Zhu et al., 2009; Shrivastava and Stevens, 2018). This approach results in irreversible losses that are indicated on the graph by the shaded area for achieving a 50% recovery (Φ_{amb}= 85%). In seawater desalination, water recovery is typically 50% (Elimelech and Phillip, 2011; Patel et al., 2020). Energy can be saved theoretically by tracking the osmotic pressure curve with an infinite cascade of RO units. This is not feasible in practice, as even the implementation of a two-stage configuration entails significant additional costs (Shrivastava and Stevens, 2018; Elimelech and Phillip, 2011). Nonetheless, the optimal pressure profile can be achieved by applying a cyclic pressure profile in a semi-batch or batch configuration. Research related to these systems has been gaining momentum. This concept looks particularly attractive for discontinuous fresh water production with DESARO compared with continuous RO in seawater desalination plants, which demand continuous high water throughput (Shrivastava and Stevens, 2018; Chougradi et al., 2021). The optimal pressure path and the average pressure over the desired permeate recovery interval can be estimated using Equation 8.

$$\pi_{av} = \frac{1}{Y}\int_0^Y \frac{\pi_0}{1-Y} dY = -\frac{\pi_0}{Y} \ln(1-Y) \quad \text{(Equation 8)}$$

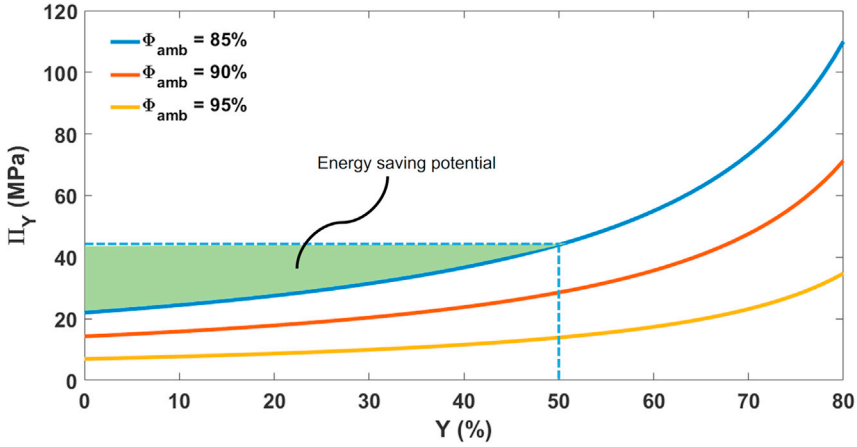

Figure 7. Osmotic pressure π_Y against the permeate water recovery Y for different initial conditions of salt solution in equilibrium with air at a relative humidity Φ_{amb}

The green shaded area indicates the energy-saving potential by following the osmotic curve (Φ_{amb} = 85%) instead of setting the outlet pressure at the desired recovery rate (Y = 50%). An ambient air temperature of 20°C is considered.

Currently, high-pressure applications of industrial reverse osmosis of seawater are operated at pressures up to 7–15 MPa, which is largely sufficient for seawater desalination (Davenport et al., 2018). Pressures of 10 MPa can be reached with hollow-fiber and spiral-wound modules. Disc-tube modules should be able to reach 20 MPa (Schantz et al., 2018). The pressures required to execute reverse osmosis of concentrated salt solutions in DESARO are even higher (Figure 8). Simulation of the DESARO process reveals that, for a process with a maximum pressure of 15 MPa, the relative humidity needs to be above 90% in the ideal case with 0% recovery and above 94% for achieving a 50% recovery. Reverse osmosis at higher pressures is needed, for instance, up to 30 MPa at 80% relative humidity or double this value at Y = 50%. Calls for higher pressures are published in the reverse osmosis literature (Schantz et al., 2018; Patel et al., 2020). The field of water-from-air extraction technologies may profit from such future technological developments in the area of reverse osmosis desalination.

Pressurizing the salt solution to force water through a semi-permeable membrane to counteract the osmotic pressure difference is the main energy input of DESARO. The specific water yield of the DESARO process is specified in Equation 9 with ρ_w the liquid water density (Sandler, 2006; Zhu et al., 2009).

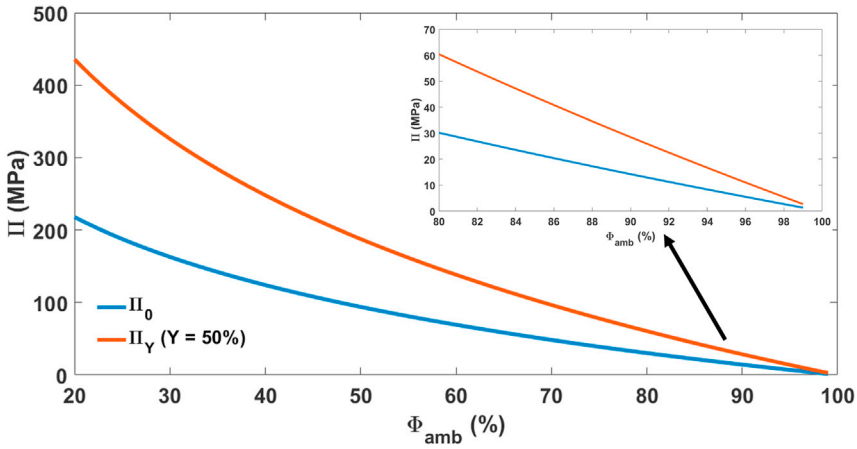

Figure 8. Minimum osmotic pressure π_0 and osmotic pressure π_Y at 50% recovery of absorbed water in the deliquescent salt reverse osmosis process plotted against relative humidity

An ambient air temperature of 20°C is considered. The inset is a zoom in the pressure range of practical interest.

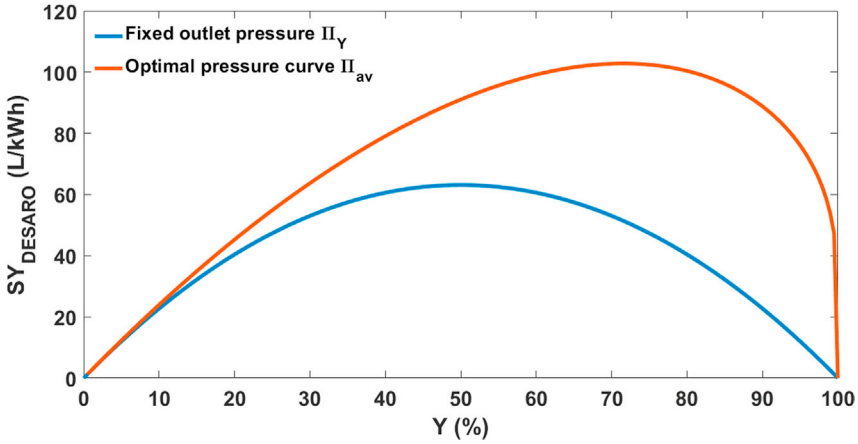

Figure 9. Specific water yield of deliquescent salt reverse osmosis SY_{DESARO} against permeate water recovery Y for a fixed outlet pressure and for variable pressure following the optimal pressure profile

An ambient air temperature of 20°C is assumed. The salt solution is in equilibrium with air at Φ_{amb} = 90% at Y = 0%.

$$SY_{DESARO} = \frac{3,600,000}{\frac{\pi}{Y\rho_w}} \quad \text{(Equation 9)}$$

For the cases $\pi = \pi_Y$ and $\pi = \pi_{av}$, the specific water yield according to this formula is plotted in Figure 9 against the water recovery Y for a salt solution in equilibrium with air at Φ_{amb} = 90%. At Y = 50%, which corresponds to the water recovery percentage typically adopted in commercial RO desalination, the maximum specific water yield is reached when the retentate outlet pressure is fixed. This means that achieving higher pressures in seawater desalination applications is not beneficial in terms of energy intensity but is merely a means to reach zero liquid discharge. The introduction of DESARO may incentivize research for high-pressure RO technology. Application of the optimal pressure profile results in a significant improvement in specific water yield and shifts the maximum to higher water recovery values (Figure 9). The possibility of recovering the pressure energy of the retentate stream with an energy recovery device was not considered in this work. Its inclusion would result in a shift of the maximum water yield to lower recovery rates (Zhu et al., 2009; Shrivastava and Stevens, 2018).

The maximum specific water yield (Equation 10) is obtained by using Equation 9 at optimal recovery Y_{opt}.

$$SY_{max,DESARO} = SY_{DESARO}(Y_{opt}) \quad \text{(Equation 10)}$$

The theoretical maximum specific water yield of the DESARO process is plotted for three cases in Figure 10. This variable is largely independent of ambient temperature but increases exponentially with relative humidity. The reason is that the water uptake of salt solutions at equilibrium increases exponentially with relative humidity. The minimum energy requirements (blue curve) are obtained by evaluating $SY_{max,DESARO}$ at the minimum pressure π_0 and by omitting Y from Equation 9 (Cengel and Boles, 2006). Deviation from this unrealistic situation leads to a significant lowering of the maximum specific water yield. The difference between the DESARO performance following the optimal pressure curve and working with a fixed pressure at Y = 50% is substantial.

Current desalination plants are operated with an efficiency of ca. 50%. Research into the energy losses has led to the conclusion that the current highly efficient pumps and energy recovery devices leave little room for further optimization. The main prospects are the development of fouling-resistant membranes to provide higher water fluxes and to reduce pre-treatment costs and total energy demand. Enhancing the membrane lifetime and the suppression of manufacturing costs are important research objectives (Shrivastava and Stevens, 2018). Mechanical stability of membranes becomes essential when operating at higher pressures to avoid membrane rupture and compaction. In addition, the corrosion resistance of equipment and the chemical stability of the membrane when using deliquescent salts are critical. Some of this salt may permeate through the membrane. The chemical nature of the salt matters since the permeation through the membrane will entail additional purification steps of the produced water.

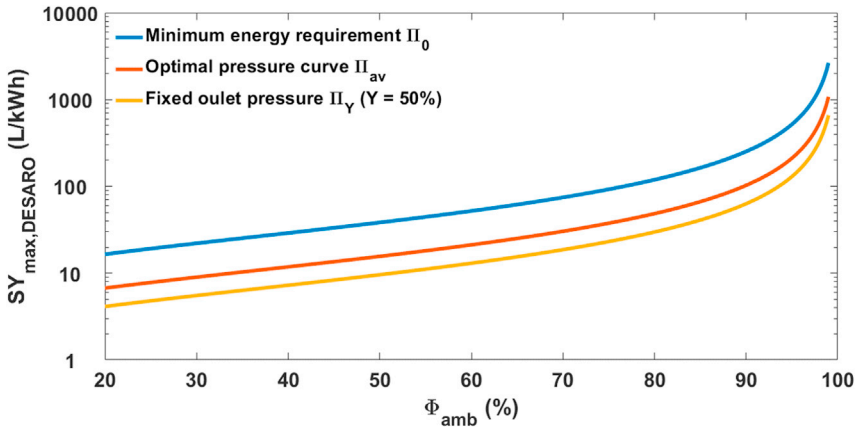

Figure 10. Maximum specific water yield of deliquescent salt reverse osmosis $SY_{max,\ DESARO}$ against relative humidity for three cases: absolute minimum energy requirements, optimal pressure profile tracking, and fixed outlet pressure

An ambient air temperature of 20°C is assumed.

Active air cooling

The proposed TRHS and DESARO processes of previous sections need to be evaluated against the simple concept for collecting airborne water by cooling air below the dew point to provoke water condensation (Figure 11). Besides the cooling, energy is also needed to force air convection by ventilation to feed the cold surface with a sufficient amount of air. In this approach, ventilation is more likely to be needed because the transported water vapor is directly condensed on the cold surfaces, whereas in the other techniques, water is captured in a separate phase of the process. The analysis of an active air cooling device is based on a reversed Carnot cycle of a coolant, known to be the most efficient refrigeration cycle (Cengel and Boles, 2006). In this device air enters the cooling unit at ambient relative humidity Φ_{amb} and temperature T_{amb}. Saturated air ($\Phi_c = 1$) and condensate leave at cooling temperature T_c (Figure 11). The derivation of the maximum specific water yield of active air cooling is moved to method details for its excessive length, which reduces readability. In this work, the passive air cooling strategies of dew and fog harvesting that occur naturally at 100% relative humidity are not considered. Locations where climate conditions are suitable for using these concepts are rare.

Estimates of the maximum specific water yield to be achieved with active cooling depending on air temperature and relative humidity, including the energy for forced convection are shown in Figure 12A. The strong increase in maximum specific water yield with relative humidity is amplified at higher temperatures (higher absolute water vapor concentrations). Sensible cooling requirements decrease at ambient relative humidity closer to 100%, and the theoretical maximum coefficient of performance increases at smaller temperature differences between the cold and hot reservoir. This relatively simple system has a major drawback, which is that at low relative humidity the dew-point temperature often will be below the freezing point causing captured water to freeze instead of condensing. It narrows substantially the operation window (Figure 12A).

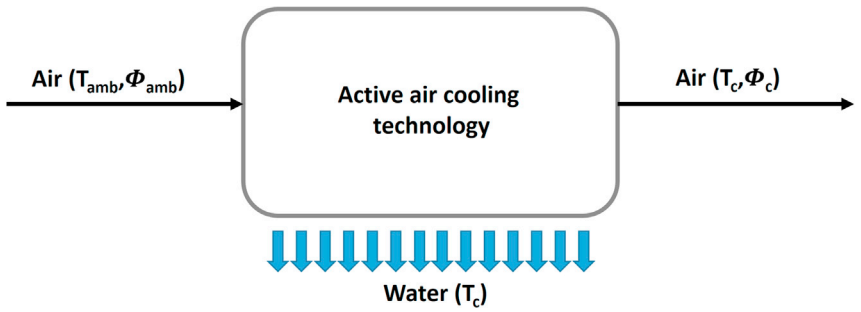

Figure 11. Active air cooling process

Inlet and outlet conditions of the active air cooling and water vapor condensation unit (Peeters et al., 2020).

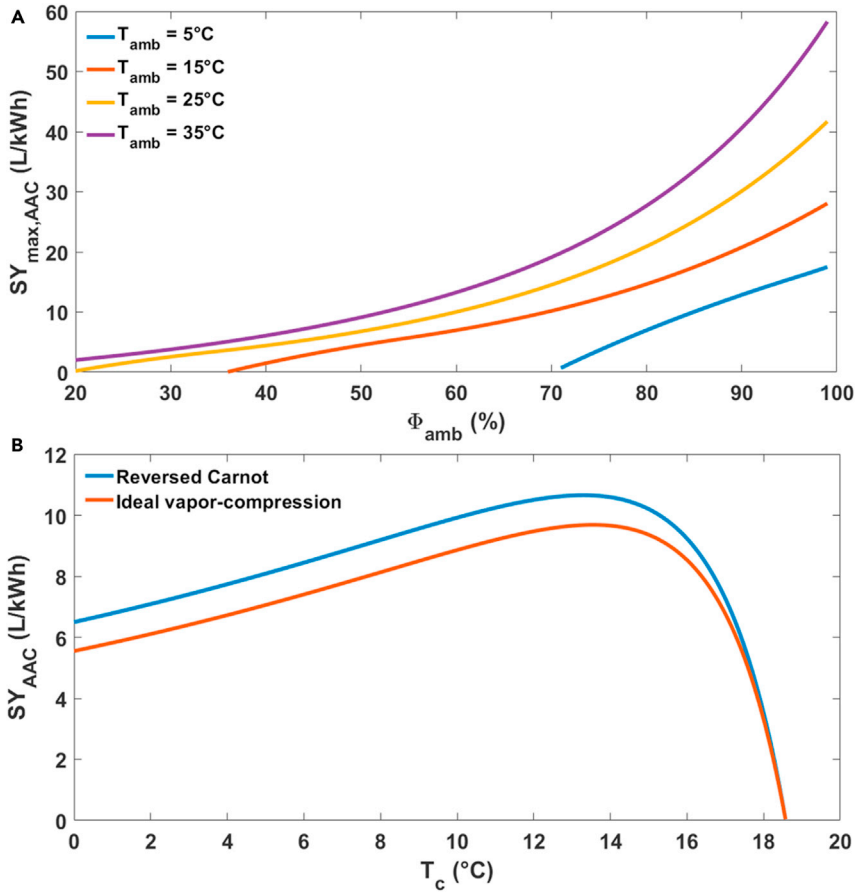

Figure 12. Specific water yield analysis of the active air cooling technology

(A) Maximum specific water yield of active air cooling $SY_{max,\ AAC}$ against relative humidity at four different temperatures (reversed Carnot cycle). The system is considered not to be applicable (zero specific water yield) when the condensation surface is below the water freezing point. Process parameter values of Table 3 are used. (B) Specific water yield of the reversed Carnot cycle and the ideal vapor-compression refrigeration cycle against the cooling temperature at $\Phi_{amb} = 60\%$ and $T_{amb} = 27°C$.

Real devices make use of a vapor-compression refrigeration cycle instead of the reversed Carnot cycle. The costly turbine of a reversed Carnot cycle is replaced by a throttling valve and the refrigerant is superheated before entering the compressor, but with the inconvenience of process irreversibilities (Cengel and Boles, 2006; Danfoss, 2010). Commercial active air cooling devices and high-efficiency dehumidifiers typically achieve specific water yields of 2–4.2 L/kWh. Such performance is generally achieved for standard conditions of 60% relative humidity at 27°C (Tu et al., 2018; Peeters et al., 2020; Talisa Water, n.d.; Watergen, n.d.; "Quest Dry 105, 155, and 205," n.d.). The specific water yield under standard conditions is plotted for the ideal reversed Carnot cycle and for the theoretical vapor-compression refrigeration cycle against the cooling temperature in Figure 12B. Abandoning the reversed Carnot cycle leads to a 10%–20% drop in maximum performance. The decrease is relatively small for cooling temperatures of interest (Danfoss, 2010). The efficiency of real processes will be lower according to the theoretical vapor-compression cycle due to non-adiabatic conditions, fluid friction, the necessary temperature differences to enable heat transfer, operation at sub-optimal cooling temperature, and the isentropic compression efficiencies, which only reach 50%–70% (Cengel and Boles, 2006; Danfoss, 2010). The most efficient dehumidifiers achieve efficiencies of at least 43% evaluated at the optimal cooling temperature in the vapor-compression cycle. Further improvements of this mature technology will probably be merely incremental.

WATER-FROM-AIR TECHNOLOGY SELECTION DEPENDING ON CLIMATE

The analysis of energy requirements of water-from-air technologies in previous sections leads to a chart indicating the energetically most favorable option depending on climate conditions (Figure 13). The

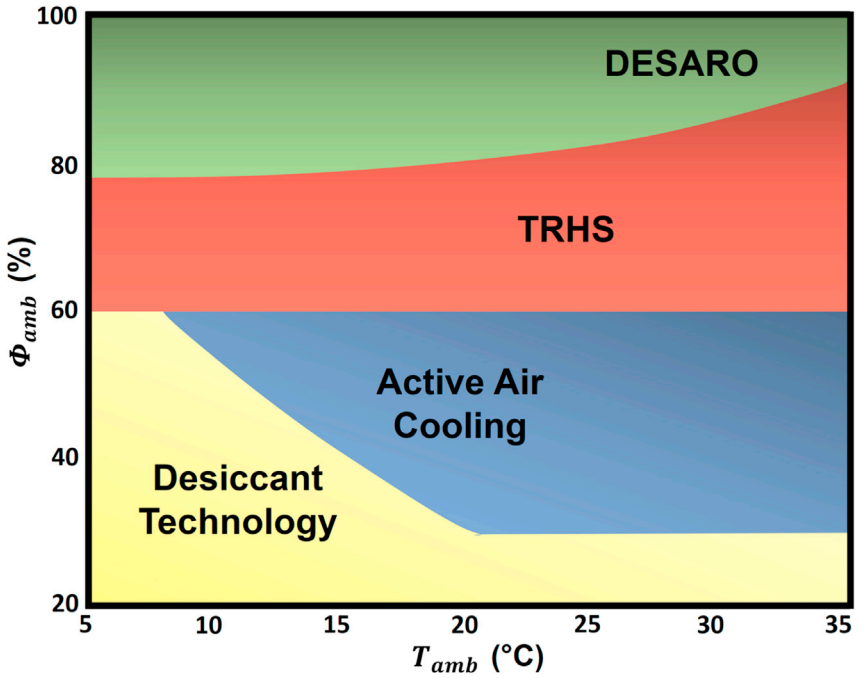

Figure 13. Preferred atmospheric water harvesting technology depending on climate conditions based on theoretical maximum specific water yields, practical considerations, and projections

Current limitations of TRHS (min. Φ_{amb} = 60%), practical considerations, and minimum energy requirements of active air cooling modeled by an ideal vapor-compression cycle (min. Φ_{amb} = 30%), and projected potential of DESARO following the optimal pressure curve (max. pressure 40 MPa) are taken into account; for desiccants, a desorption enthalpy of 3,300,000 J/kg is considered.

DESARO process is the best choice at high relative humidity. This process was modeled using the optimal pressure profile for a permeate water recovery that maximizes the specific water yield without exceeding a maximum pressure of 40 MPa, which represents a realistic maximum pressure that the membrane could withstand (Killian Mcgovern et al., 2015).

Thermo-responsive polymers (TRHS) are the best candidates at high-mid relative humidity conditions. Currently, the concept has been demonstrated at relative humidities above 60% (Figure 13) (Zhao et al., 2019). The imposed lower boundary can be lowered in the future when the operability at lower relative humidity is enhanced by improvements in the polymer design and reduction of evaporation losses.

Low relative humidity typically coincides with high temperatures, like in deserts. In these conditions, active air cooling seems to be the best choice (Figure 13). This method was modeled by the vapor-compression refrigeration cycle. A minimum operational relative humidity of 30% is imposed, which acts as a compromise between a minimum of 20% calculated by the model when operating at the optimal cooling temperature and a minimum of 40% given as practical advice for choosing between an active cooling and desiccant-based dehumidifier (Condair, 2016). At lower temperatures or at extremely low relative humidity, desiccant-based technology becomes the favored option.

The active air cooling approach for capturing water vapor is similar to commercially well-established dehumidifiers and air conditioners. At low relative humidity, most energy goes to the cooling of gases composing the air next to water vapor (Gido et al., 2016a). Cold air from the process outlet can be utilized to pre-cool the ambient air stream to increase the inlet relative humidity (Gido et al., 2016b). Another alternative is the implementation of a water-selective membrane prior to the cooling step to increase the inlet relative humidity of the cooling device (Bergmair et al., 2014). DESARO could also be combined with active air cooling. The water vapor from the cold saturated outlet air (Φ = 100%) could be liquefied by deliquescent salts and subsequently separated by reverse osmosis at a low energy cost.

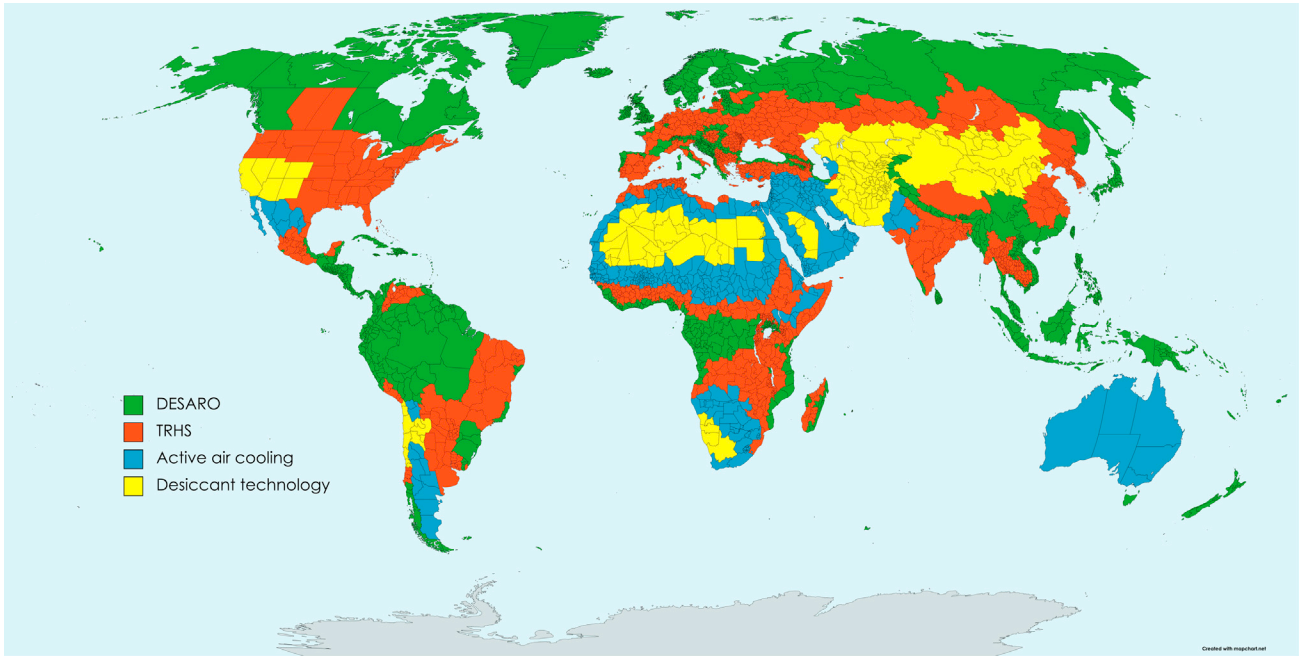

Figure 14. World map showing the preferred local water-from-air technology

Figure made with Mapchart.net ("MapChart," n.d.). The world map is constructed by using climate data from Figure S1. The world map of water-from-air technologies is based on the highest theoretical maximum specific water yields according to the local climate and additional technological constraints (see Figure 13).

The optimal technology depending on climate conditions (Figure 13) is implemented on the world map in Figure 14. Details of the world map construction based on yearly average relative humidity during the night and annual average ambient temperature (Figure S1) can be found in supplemental information (Hersbach et al., 2019a, 2019b). Relative humidities of 20%–40% are common in North Africa, the Middle East, and Australia. These low values coincide with high temperatures between 20°C and 30°C. In those locations where desiccant-based technology or active air cooling is advised, the best choice depends on more accurate local climate data. Relative humidities between 40% and 60% (0°C–20°C) are prevailing in parts of Asia and warm locations close to coastlines. Active air cooling is preferred in these areas for the higher relative humidity and temperature cases and desiccant-based technology for the drier and colder parts of these regions. Large parts of Europe, North and South America, and India have mild climates with relative humidities of 60%–80%, which is ideal for the TRHS polymer approach (Figure 13). Locations around the Equator, islands like New Zealand and the Caribbean, and cold regions far North are characterized by very high relative humidities above 80%. The DESARO technology is advised in these areas when technological maturity is reached.

ATMOSPHERIC WATER HARVESTING AND THE LOCAL WATER-ENERGY NEXUS

In the analyses of the maximum specific water yields abstraction was made regarding the origin of the energy source. In practice, this choice affects the water-energy nexus. The desiccant-based technology does not affect the water-energy nexus when using solar heating, but the modest specific water yield translates into large surface area requirements (Zhou et al., 2020a; LaPotin et al., 2019). An active desiccant approach using electrical heating solves the spatial requirements, but the resulting water consumption of the energy technology may overshadow the specific water yield of the desiccant device. Execution of the final cooling step of the desiccant-based water harvesting cycle may not be effective at high ambient temperatures, resulting in the implementation of an external electrically powered cooling device. Similar to the refrigeration-based cooling principle of the active air cooling process, the electricity demand can result in a significant reduction of the net specific water yield and thereby negatively impact the water-energy nexus (Peeters et al., 2020).

The TRHS approach can take advantage of the availability of abundant solar energy as well. The captured water can be instantly released at the desired location during the day by solar heating, which

removes the condensation step. It avoids the need for a water distribution network and a specific delivery device, making it ideal for direct irrigation (Zhou et al., 2020b). The high specific water yield reduces the impact of water consumption in the energy sector if use is made of a man-made energy source for heating.

The operation of DESARO will likely be executed in large plants. The mechanical pressure-driven process needs electricity to function. The source of electricity production is therefore of importance. A comparable effect on the water-energy nexus as seawater desalination is expected when operating at high relative humidity.

Water can be provided to various industries and sectors with water-from-air technologies, provided that the specific water yield is higher than the water consumption for the production of the energy needed for the water capturing process. In addition to the direct implementation of these technologies for capturing atmospheric water, fresh water can be produced as a side product of, e.g., heating, ventilation, and air conditioning (HVAC) systems (Raveesh et al., 2021; Magrini et al., 2017). Approximately 40% of the evaporated water from cooling towers can easily be captured with fog collection mesh structures (Raveesh et al., 2021; Ghosh et al., 2015). The technology behind high-pressure RO enables water recovery from hypersaline waste from, e.g., the textile industry or landfill leachate streams with reduced energy (Davenport et al., 2018). Water losses by evaporation can also be recovered efficiently by TRHS polymers in industrial plants when sufficient waste heat is available.

WATER FROM AIR VERSUS FRESH WATER PRODUCTION FROM LIQUID WATER SOURCES

Water production from the air and from traditional liquid water sources involve different unit operations and have largely different energy needs (Figure 15). For the water-from-air technologies in Figure 15, the theoretical maximum specific water yield is represented with the black boxes and evaluated at various conditions highlighted in the figure caption. Actual performances extracted from literature data (blue boxes) evidently do not reach the theoretical maxima. DESARO presently is only a concept and not yet applied. It is most promising since in principle at high relative humidity it could reach the energy performance of seawater desalination. A detailed explanation of the performances and achieved efficiencies can be found in the corresponding technology sections already presented.

Among the technologies for the production of fresh water starting from liquid water sources (right side of Figure 15), reverse osmosis has the highest energy efficiency among seawater desalination technologies (Deshmukh et al., 2018). This pressure-driven fresh water production process achieves a specific water yield of around 250–500 L/kWh depending on initial and final salt concentrations (IEA, 2016; Shrivastava and Stevens, 2018; Elimelech and Phillip, 2011; Memon and Ward, 2014). Avoiding phase transition by mechanical-based separation takes less energy compared with thermal processes, greatly reducing energy costs (Shrivastava and Stevens, 2018; Schantz et al., 2018; Wu et al., 2021). Wastewater purification with biological and physicochemical means is a very energy-efficient way of fresh water production. The energy consumption of wastewater treatment depends on the inlet quality of the water and the desired end quality. In general, the specific water yield is higher than for desalination. A decentralized rainwater harvesting system essentially needs energy for pumping water in and out of reservoirs. A buffer system has to be foreseen to cope with the intermittency of rainfall (Memon and Ward, 2014). Large-scale water production from surface and underground reservoirs are the least energy-intensive water production technologies (IEA, 2016). Fresh water production from groundwater and surface water sources are the basic supply options, but gradually more wastewater treatment facilities have been constructed to deal with the deterioration of water quality. The next step in this intensification process was the increase in seawater desalination capacity, especially observed in regions like the Middle East (IEA, 2016). A large gap is observed between actual water-from-air technologies and fresh water production from liquid water sources (Figure 15). The theoretical limits are much closer, especially for DESARO. Atmospheric water capturing technologies involving only one phase transition of water (TRHS, DESARO, and active cooling) energy-wise pose the logical next step in water supply technologies.

Purely on an energy basis, water-from-air technologies are not competitive with conventional water production from liquid sources. However, harvesting omnipresent atmospheric water vapor becomes a viable option in the absence of natural fresh water sources. In such cases, decentralized water production from the air has to be compared on a total cost basis with centralized fresh water production in combination with

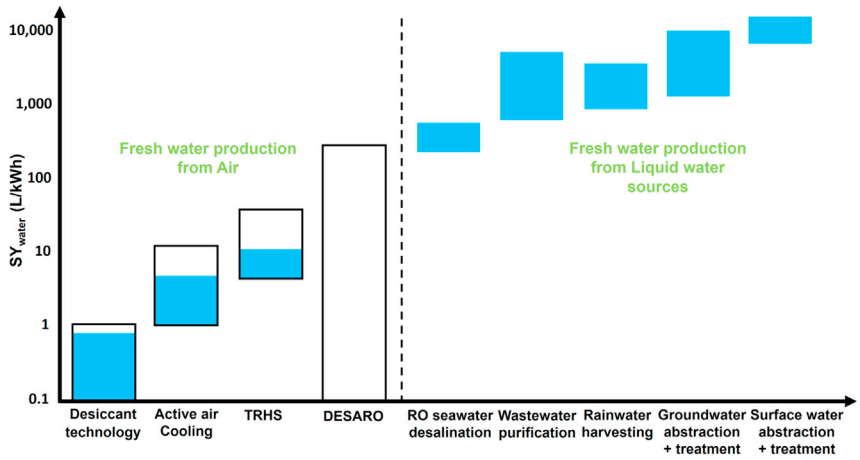

Figure 15. Specific water yield of fresh water production technologies

Specific water yield SY_{water} of water-from-air technologies (left) and fresh water supply technologies from natural liquid water sources (right). Black boxes: theoretical maximum values of desiccant technology ($SY_{max,water} = 1\ L/kWh$), active air cooling with ideal vapor-compression cycle evaluated at $\Phi_{amb} = 60\%$ and $T_{amb} = 27°C$, TRHS evaluated at $\Phi_{amb} = 90\%$ and $T_{amb} = 25°C$, and DESARO with pressure curve tracking evaluated at optimal water recovery at $\Phi_{amb} = 95\%$ and $T_{amb} = 20°C$; blue boxes: literature values (IEA, 2016; Peeters et al., 2020; Zhao et al., 2019; Li et al., 2018; "Quest Dry 105, 155, and 205," n.d.; Memon and Ward, 2014).

long-distance transport. Constructing pipeline networks connected to water production facilities like seawater desalination plants may not be an option for small communities by the high upfront capital expenditures. Political and societal aspects may also complicate the option of long-distance transportation building a case for water-from-air technologies.

Water production will become increasingly expensive, especially when the traditional liquid water reserves become exhausted. Seawater desalination is more energy demanding by at least one order of magnitude compared with water production from wastewater, natural precipitation, and surface and underground fresh water reserves. Water-from-air technologies will again be at least ten times more energy demanding.

CONCLUSIONS AND OUTLOOK

Analysis of the theoretical maximum specific water yield reveals the potential for established and new water-from-air extraction processes and provides a basis for making choices depending on climate conditions. Two relatively new concepts, the temperature-responsive hydrophilicity switching polymers (TRHS) and DESARO involving only one phase transition of water, energetically score very well and approach the energy performances of water production from liquid water sources. For the DESARO process being theoretically most energy-efficient among the water-from-air technologies, the practical implementation will be largely dependent on future developments of high-pressure reverse osmosis technology, which will expand the relative humidity range where high specific water yields can be realized. Especially the development of a mechanical and chemical stable water permeable membrane withstanding high pressure is a grand challenge. Successful implementation of the DESARO process critically depends on the selection of a deliquescent salt with limited corrosivity and that remains liquid throughout the process. TRHS polymers dedicated to this field of water-from-air extraction technologies are needed. Improving the water uptake and achieving a large water capacity at low relative humidity are required to produce large quantities of water at a low energy cost. Efficient use of TRHS polymers will critically depend on the design of processes maximizing the intrinsic advantages of this technology. The optimum climate conditions for DESARO and TRHS technologies are limited to mid-high relative humidity. For arid regions of the world, desiccant-based technologies and active cooling to provoke condensation are advised, but these techniques are very energy intensive. Research on adsorbents for desiccant technologies has already been very successful, and actual performances are close to the thermodynamic limits. The successful development of adsorption processes may incentivize research on the alternative concepts needed for water harvesting regions with milder climates.

METHOD DETAILS

The derivation of the maximum specific water yield of active air cooling is given in this section.

Active air cooling

A graphical representation of the active air cooling approach is provided in Figure 11. The difference in absolute humidity of inlet and outlet air ($\omega_{amb} - \omega_c$) and the air volume defines the amount of extracted water. The relation between relative humidity (Φ), absolute humidity (ω), total air pressure (P), and temperature (T) is used to determine the absolute humidity at the inlet and outlet states of air (Equation 11) (Peeters et al., 2020; Cengel and Boles, 2006).

$$\Phi = \frac{\omega P}{(0.622 + \omega) P_s(T)} \quad \text{(Equation 11)}$$

The total pressure P equals the sum of dry air pressure (P_a) and water vapor pressure (P_w). The dry air pressure is set at 100,000 Pa. The water vapor pressure P_w is obtained from an alternative representation of relative humidity (Equation 12) (Peeters et al., 2020; Cengel and Boles, 2006).

$$\Phi = \frac{P_w}{P_s(T)} \quad \text{(Equation 12)}$$

The water vapor saturation pressure P_s is obtained from Equation 13 with the temperature T in °C (Alduchov and Eskridge, 1996).

$$P_s(T) = 610.94 exp\left(\frac{17.625T}{243.04 + T}\right) \quad \text{(Equation 13)}$$

Two main energy contributions are included in the denominator of the maximum specific water yield equation of active air cooling $SY_{max,\ AAC}$ (Equation 14). Cooling requirements are estimated from the difference in air enthalpy at ambient conditions (H_{amb}) and the enthalpies of the two outlet streams: air evaluated at cooling temperature (H_c) and the enthalpy of extracted liquid water (H_L).

$$SY_{max,\ AAC} = \frac{3,600,000}{\frac{H_{amb} - (H_c + H_L)}{COP_{cooling}(\omega_{amb} - \omega_c)} + \frac{\dot{P}_v}{\rho_a \dot{V}_a (\omega_{amb} - \omega_c)}} \quad \text{(Equation 14)}$$

The enthalpy of water-bearing air is given in Equation 15, and the enthalpy of liquid water in Equation 16. $C_{p,a}$ and $C_{p,wv}$ represent the heat capacity of dry air and the heat capacity of water vapor, respectively (Peeters et al., 2020; Cengel and Boles, 2006).

$$H_i = C_{p,a} T_i + \omega (H_{wv}(0°C) + C_{p,wv} T_i) \quad \text{(Equation 15)}$$

$$H_L = (\omega_{amb} - \omega_c) C_{p,w} T_c \quad \text{(Equation 16)}$$

The coefficient of performance of a cooling device $COP_{cooling}$ that follows a reversed Carnot cycle is shown in Equation 17 (Peeters et al., 2020; Cengel and Boles, 2006).

$$COP_{cooling} = \frac{T_c}{T_{amb} - T_c} \quad \text{(Equation 17)}$$

The maximum specific water yield of active air cooling $SY_{max,\ AAC}$ (Equation 14) includes ventilation power consumption, which is incorporated in the second term of the denominator with the air density ρ_a, the volumetric airflow rate $\dot{V}_a$, and the fan power consumption $\dot{P}_v$. The cooling temperature T_c is chosen as the optimal temperature which maximizes the specific water yield and ranges from 0°C to the dew-point temperature. Temperatures below the freezing point of water are omitted from the analysis (Peeters et al., 2020). Parameter values used in the analysis are included in Table 3.

The efficiency of a theoretical vapor-compression refrigeration cycle is obtained by multiplying $COP_{cooling}$ by the Carnot efficiency η_c. A realistic and approximated value that is valid for a variety of refrigerants can be calculated by using Equation 18 for a single-stage cycle (Danfoss, 2010). This correlation was constructed for a hot reservoir temperature of 30°C which is close to the standardized temperature of 27°C used to calculate the performance of commercial active cooling devices.

$$\eta_c = 0.0035 T_c + 0.85 \quad \text{(Equation 18)}$$

Table 3. Parameter values used for estimating the maximum specific water yield of active air cooling

Parameter	Value	Reference
$C_{p,w}$	4,185 J/kg.K	(Incropera et al., 2013)
$C_{p,a}$	1,005 J/kg.°C	(Cengel and Boles, 2006)
$C_{p,wv}$	1,820 J/kg.°C	(Cengel and Boles, 2006)
$H_{wv}(0°C)$	2,500,900 J/kg	(Cengel and Boles, 2006)
$\dot{P}_v$	140 W	(Blauberg Ventilatoren, 2017)
$\dot{V}_a$	0.7 m^3/s	(Blauberg Ventilatoren, 2017)
ρ_a	1.25 kg/m^3	(Incropera et al., 2013)

The mathematic code to calculate the specific water yields of water-from-air technologies is made publicly available at Harvard Dataverse (https://doi.org/10.7910/DVN/GV0HIJ).

Limitations of the study

The world map showing the preferred local water-from-air technology is based on averages concerning ambient relative humidity and temperature. Taking into account daily fluctuations and seasonal shifts in climate conditions would result in a time-dependent optimal technology choice. The provided world map only serves as a general indication of the potential of each technology.

SUPPLEMENTAL INFORMATION

Supplemental information can be found online at https://doi.org/10.1016/j.isci.2021.103266.

ACKNOWLEDGMENTS

The authors acknowledge European Research Council (ERC) under the European Union's Horizon 2020 research and innovation program, WATUSO (grant agreement No. [834134]) financial support, and the Flemish Government for long-term structural funding (Methusalem funding METH/14/04).

This work contains modified Copernicus Climate Change Service information [2018, 2019, 2020]. Neither the European Commission nor ECMWF is responsible for any use that may be made of the Copernicus information or data it contains. The specific datasets of Hersbach et al. (2019a, 2019b) were used.

We like to thank Yi-Sheng Wang for creating the world map of relative humidity and temperature conditions (Figure S1).

The world map with optimal atmospheric water harvesting technologies (Figure 14) was created with Mapchart.net (licensed under a Creative Commons Attribution-ShareAlike 4.0 International License).

AUTHOR CONTRIBUTIONS

Conceptualization, R.P. and J.A.M.; methodology, R.P.; writing – original draft, R.P. and H.V.; writing – review & editing, R.P., H.V., J.R., and J.A.M.; supervision, J.R. and J.A.M.; funding acquisition, J.A.M.

DECLARATION OF INTERESTS

The authors declare no competing interests.

REFERENCES

Afroze, F., Nies, E., and Berghmans, H. (2000). Phase transitions in the system poly(N-isopropylacrylamide)/water and swelling behaviour of the corresponding networks. J. Mol. Struct. *554*, 55–68. https://doi.org/10.1016/S0022-2860(00)00559-7.

Akbar Salehi, A., Ghannadi-maragheh, M., Torab-mostaedi, M., Torkaman, R., and Asadollahzadeh, M. (2020). A review on the water-energy nexus for drinking water production from humid air. Renew. Sustain. Energy Rev. *120*, 109627. https://doi.org/10.1016/j.rser.2019.109627.

Alayli, Y., Hadji, N.E., and Lebond, J. (1987). A New Process for the extraction of water from air. Desalination *67*, 227–229.

Alduchov, O.A., and Eskridge, R.E. (1996). Improved magnus form approximation of saturation vapor pressure. J. Appl. Meteorol. *35*, 601–609.

Asim, N., Badiei, M., Alghoul, M.A., Mohammad, M., Samsudin, N.A., Amin, N., and Sopian, K. (2021). Sorbent-based air water-harvesting systems: progress, limitation, and consideration.

Rev. Environ. Sci. Biotechnol. *20*, 257–279. https://doi.org/10.1007/s11157-020-09558-6.

Bergmair, D., Metz, S.J., de Lange, H.C., and van Steenhoven, A.A. (2014). System analysis of membrane facilitated water generation from air humidity. Desalination *339*, 26–33. https://doi.org/10.1016/j.desal.2014.02.007.

Blauberg Ventilatoren. (2017). Industrial ventilation. https://blaubergventilatoren.de/uploads/download/blcatalogueind201701en.pdf.

Cantrell, W., McCrory, C., and Ewing, G.E. (2002). Nucleated deliquescence of salt. J. Chem. Phys. *116*, 2116–2120. https://doi.org/10.1063/1.1429924.

Cengel, Y.A., and Boles, M.A. (2006). Thermodynamics an Engineering Approach, 5th Edition (McGraw-Hill).

Chakraborty, A., Saha, B.B., and Koyama, S. (2009). Adsorption thermodynamics of silica gel-water systems. J. Chem. Eng. Data *54*, 448–452. https://doi.org/10.1021/je800458k.

Chapagain, A.K., and Hoekstra, A.Y. (2004). Water Footprints of Nations, Value of Water Research Report Series No. 16 (Unesco-IHE Institute for Water Education).

Chougradi, A., Zaviska, F., Abed, A., Harmand, J., Jellal, J.E., and Heran, M. (2021). Batch reverse osmosis desalination modeling under a time-dependent pressure profile. Membranes *11*, 173. https://doi.org/10.3390/membranes11030173.

Condair. (2016). Dehumidification Planning guidelines for technical building services and specialist planners. https://www.condair.dk/m/0/planningbrochure-dehumidification-161018-en.pdf.

Coronado, R., Pekerar, S., Lorenzo, A.T., and Sabino, M.A. (2011). Characterization of thermo-sensitive hydrogels based on poly(N-isopropylacrylamide)/hyaluronic acid. Polym. Bull. *67*, 101–124. https://doi.org/10.1007/s00289-010-0407-6.

Danfoss. (2010). Thermodynamic Limitations and Opportunities for Reaching High Energy-Efficient Refrigeration, Heat Pump and Air Conditioning Systems (Danfoss A/S).

Davenport, D.M., Deshmukh, A., Werber, J.R., and Elimelech, M. (2018). High-pressure reverse osmosis for energy-efficient hypersaline brine desalination: current status, design considerations, and research needs. Environ. Sci. Technol. Lett. *5*, 467–475. https://doi.org/10.1021/acs.estlett.8b00274.

Davila, A.F., Duport, L.G., Melchiorri, R., Jänchen, J., Valea, S., De Los Rios, A., Fairén, A.G., Möhlmann, D., McKay, C.P., Ascaso, C., and Wierzchos, J. (2010). Hygroscopic salts and the potential for life on mars. Astrobiology *10*, 617–628. https://doi.org/10.1089/ast.2009.0421.

Deshmukh, A., Boo, C., Karanikola, V., Lin, S., Straub, A.P., Tong, T., Warsinger, D.M., and Elimelech, M. (2018). Membrane distillation at the water-energy nexus: limits, opportunities, and challenges. Energy Environ. Sci. *11*, 1177–1196. https://doi.org/10.1039/C8EE00291F.

Ejeian, M., Entezari, A., and Wang, R.Z. (2020). Solar powered atmospheric water harvesting with enhanced LiCl/MgSO4/ACF composite. Appl. Therm. Eng. *176*, 115396. https://doi.org/10.1016/J.APPLTHERMALENG.2020.115396.

Elashmawy, M. (2020). Experimental study on water extraction from atmospheric air using tubular solar still. J. Clean. Prod. *249*, 119322. https://doi.org/10.1016/j.jclepro.2019.119322.

Elimelech, M., and Phillip, W.A. (2011). The future of seawater desalination: Energy, technology, and the environment. Science *333*, 712–717. https://doi.org/10.1126/science.1200488.

Entezari, A., Ejeian, M., and Wang, R. (2020). Super atmospheric water harvesting hydrogel with alginate chains modified with binary salts. ACS Mater. Lett. *2*, 471–477. https://doi.org/10.1021/acsmaterialslett.9b00315.

Fathieh, F., Kalmutzki, M.J., Kapustin, E.A., Waller, P.J., Yang, J., and Yaghi, O.M. (2018). Practical water production from desert air. Sci. Adv. *4*, eaat3198. https://doi.org/10.1126/sciadv.aat3198.

Gad, H.E., Hamed, A.M., and El-Sharkawy, I.I. (2001). Application of a solar desiccant/collector system for water recovery from atmospheric air. Renew. Energy *22*, 541–556.

Ghosh, R., Ray, T.K., and Ganguly, R. (2015). Cooling tower fog harvesting in power plants – a pilot study. Energy *89*, 1018–1028. https://doi.org/10.1016/J.ENERGY.2015.06.050.

Gido, B., Friedler, E., and Broday, D.M. (2016a). Liquid-desiccant vapor separation reduces the energy requirements of atmospheric moisture harvesting. Environ. Sci. Technol. *50*, 8362–8367. https://doi.org/10.1021/acs.est.6b01280.

Gido, B., Friedler, E., and Broday, D.M. (2016b). Assessment of atmospheric moisture harvesting by direct cooling. Atmos. Res. *182*, 156–162. https://doi.org/10.1016/j.atmosres.2016.07.029.

Hanikel, N., Prévot, M.S., Fathieh, F., Kapustin, E.A., Lyu, H., Wang, H., Diercks, N.J., Glover, T.G., and Yaghi, O.M. (2019). Rapid cycling and exceptional yield in a metal-organic framework water harvester. ACS Cent. Sci. *5*, 1699–1706. https://doi.org/10.1021/acscentsci.9b00745.

Hersbach, H., Bell, B., Berrisford, P., Biavati, G., Horányi, A., Muñoz Sabater, J., Nicolas, J., Peubey, C., Radu, R., Rozum, I., et al. (2019a). ERA5 monthly averaged data on single levels from 1979 to present. Copernicus Climate Change Service (C3S) Climate Data Store (CDS). https://doi.org/10.24381/cds.f17050d7.

Hersbach, H., Bell, B., Berrisford, P., Biavati, G., Horányi, A., Muñoz Sabater, J., Nicolas, J., Peubey, C., Radu, R., Rozum, I., et al. (2019b). ERA5 monthly averaged data on pressure levels from 1979 to present. Copernicus Climate Change Service (C3S) Climate Data Store (CDS). https://doi.org/10.24381/cds.6860a573.

Hua, L., Xu, J., and Wang, R. (2021). Exergy-efficient boundary and design guidelines for atmospheric water harvesters with nano-porous sorbents. Nano Energy *85*, 105977. https://doi.org/10.1016/j.nanoen.2021.105977.

IEA (2016). Water Energy Nexus- Excerpt from the World Energy Outlook 2016 (International Energy Agency).

Incropera, F.P., Dewitt, D.P., Bergman, T.L., and Lavine, A.S. (2013). Principles of Heat and Mass Transfer, 7th Edition (Wiley).

Jarimi, H., Powell, R., and Riffat, S. (2020). Review of sustainable methods for atmospheric water harvesting. Int. J. Low-Carbon Technol. *15*, 253–276. https://doi.org/10.1093/ijlct/ctz072.

Kallenberger, P.A., and Fröba, M. (2018). Water harvesting from air with a hygroscopic salt in a hydrogel–derived matrix. Commun. Chem. *1*, 28. https://doi.org/10.1038/s42004-018-0028-9.

Karmakar, A., Mileo, P.G.M., Bok, I., Peh, S.B., Zhang, J., Yuan, H., Maurin, G., and Zhao, D. (2020). Thermo-responsive MOF/polymer composites for temperature-mediated water capture and release. Angew. Chem. Int. Ed. *59*, 11003–11009. https://doi.org/10.1002/anie.202002384.

Killian Mcgovern, R., Mcconnon, D., and Lienhard, J.H. (2015). The effect of very high hydraulic pressure on the permeability and salt rejection of reverse osmosis membranes. IDA. World Congr. Desalin. Water Reuse, 1–7.

Kim, H., Cho, H.J., Narayanan, S., Yang, S., Furukawa, H., Schiffres, S., Li, X., Zhang, Y.B., Jiang, J., Yaghi, O.M., and Wang, E.N. (2016). Characterization of adsorption enthalpy of novel water-stable zeolites and metal-organic frameworks. Sci. Rep. *6*, 19097. https://doi.org/10.1038/srep19097.

Kim, H., Rao, S.R., Kapustin, E.A., Zhao, L., Yang, S., Yaghi, O.M., and Wang, E.N. (2018). Adsorption-based atmospheric water harvesting device for arid climates. Nat. Commun. *9*, 1191. https://doi.org/10.1038/s41467-018-03162-7.

Kim, H., Yang, S., Rao, S.R., Narayanan, S., Kapustin, E.A., Furukawa, H., Umans, A.S., Yaghi, O.M., and Wang, E.N. (2017). Water harvesting from air with metal-organic frameworks powered by natural sunlight. Science *356*, 430–434. https://doi.org/10.1126/science.aam8743.

LaPotin, A., Kim, H., Rao, S.R., and Wang, E.N. (2019). Adsorption-based atmospheric water harvesting: impact of material and component properties on system-level performance. Acc. Chem. Res. *52*, 1588–1597. https://doi.org/10.1021/acs.accounts.9b00062.

LaPotin, A., Zhong, Y., Zhang, L., Zhao, L., Leroy, A., Kim, H., Rao, S.R., and Wang, E.N. (2021). Dual-stage atmospheric water harvesting device for scalable solar-driven water production. Joule *5*, 166–182. https://doi.org/10.1016/J.JOULE.2020.09.008.

Lee, U., Han, J., and Elgowainy, A. (2016). Water Consumption Factors for Electricity Generation in the United States.

Li, R., Shi, Y., Alsaedi, M., Wu, M., Shi, L., and Wang, P. (2018). Hybrid hydrogel with high water vapor harvesting capacity for deployable solar-driven atmospheric water generator. Environ. Sci. Technol. *52*, 11367–11377. https://doi.org/10.1021/acs.est.8b02852.

Li, R., Shi, Y., Wu, M., Hong, S., and Wang, P. (2020). Improving atmospheric water production yield: Enabling multiple water harvesting cycles with nano sorbent. Nano Energy *67*, 104255. https://doi.org/10.1016/j.nanoen.2019.104255.

Linnow, K., Niermann, M., Bonatz, D., Posern, K., and Steiger, M. (2014). Experimental studies of the mechanism and kinetics of hydration reactions. Energy Proced. *48*, 394–404. https://doi.org/10.1016/j.egypro.2014.02.046.

Magrini, A., Cattani, L., Cartesegna, M., and Magnani, L. (2017). Water production from air conditioning systems: Some evaluations about a sustainable use of resources. Sustainability *9*, 1309. https://doi.org/10.3390/su9081309.

MapChart. https://mapchart.net/index.html.

Matsumoto, K., Sakikawa, N., and Miyata, T. (2018). Thermo-responsive gels that absorb moisture and ooze water. Nat. Commun. *9*, 2315. https://doi.org/10.1038/s41467-018-04810-8.

Mauer, L.J., and Taylor, L.S. (2010). Water-solids interactions: deliquescence. Annu. Rev. Food Sci. Technol. *1*, 41–63. https://doi.org/10.1146/annurev.food.080708.100915.

Mekonnen, M.M., and Hoekstra, A.Y. (2011). National water footprint accounts: the green, blue and grey water footprint of production and consumption, Value of Water Research Report Series No. 50. Delft, The Netherlands. https://doi.org/10.5194/hessd-8-763-2011.

Memon, F.A., and Ward, S. (2014). Alternative Water Supply Systems (IWA Publishing. IWA Publishing). https://doi.org/10.2166/9781780405513.

Mulchandani, A., Malinda, S., Edberg, J., and Westerhoff, P. (2020). Sunlight-driven atmospheric water capture capacity is enhanced by nano-enabled photothermal desiccants. Environ. Sci. Nano *7*, 2584–2594. https://doi.org/10.1039/d0en00463d.

Patel, S.K., Ritt, C.L., Deshmukh, A., Wang, Z., Qin, M., Epsztein, R., and Elimelech, M. (2020). The relative insignificance of advanced materials in enhancing the energy efficiency of desalination technologies. Energy Environ. Sci. *13*, 1694. https://doi.org/10.1039/d0ee00341g.

Peeters, R., Vanderschaeghe, H., Rongé, J., and Martens, J.A. (2020). Energy performance and climate dependency of technologies for fresh water production from atmospheric water vapour. Environ. Sci. Water Res. Technol. *6*, 2016–2034. https://doi.org/10.1039/d0ew00128g.

Quest dry 105, 155, and 205. https://www.questclimate.com/pdf/Quest-Dry-105-155-205-Manual.pdf.

Rautenbach, R., and Linn, T. (1996). High-pressure Reverse Osmosis and Nanofiltration , a " Zero Discharge " Process Combination for the Treatment of Waste Water with Severe Fouling/Scaling Potential, *105*, pp. 63–70.

Raveesh, G., Goyal, R., and Tyagi, S.K. (2021). Advances in atmospheric water generation technologies. Energy Convers. Manag. *239*, 114226. https://doi.org/10.1016/j.enconman.2021.114226.

Sandler, S.I. (2006). Chemical, Biochemical, and Engineering Thermodynamics, 4th Edition (Wiley).

Schantz, A.B., Xiong, B., Dees, E., Moore, D.R., Yang, X., and Kumar, M. (2018). Emerging investigators series: prospects and challenges for high-pressure reverse osmosis in minimizing concentrated waste streams. Environ. Sci. Water Res. Technol. *4*, 894–908. https://doi.org/10.1039/c8ew00137e.

Shiklomanov, I.A. (1993). World's fresh water resources. In Water in Crisis A Guide to the World's Fresh Water Resources, P.H. Gleick, ed. (Oxford University Press), pp. 13–24.

Shrivastava, A., and Stevens, D. (2018). Energy efficiency of reverse osmosis. In Sustainable Desalination Handbook, pp. 25–54. https://doi.org/10.1016/B978-0-12-809240-8.00002-2.

Sleiti, A.K., Al-Khawaja, H., Al-Khawaja, H., and Al-Ali, M. (2021). Harvesting water from air using adsorption material – Prototype and experimental results. Sep. Purif. Technol. *257*, 117921. https://doi.org/10.1016/j.seppur.2020.117921.

Takigawa, T., Takahashi, K., and Aki, H.A.R. (2001). Transition enthalpy for a poly (N-isopropylacrylamide) based polymer gel. Polym. J. *33*, 297–300.

Talisa Water. ECOLOBLUE 1000 industrial atmospheric water generator. https://talisa.co.za/ecoloblue-1000-i/.

Tereshchenko, A.G. (2015). Deliquescence: Hygroscopicity of water-soluble crystalline solids. J. Pharm. Sci. *104*, 3639–3652. https://doi.org/10.1002/jps.24589.

Tu, Y., Wang, R., Zhang, Y., and Wang, J. (2018). Progress and expectation of atmospheric water harvesting. Joule *2*, 1452–1475. https://doi.org/10.1016/J.JOULE.2018.07.015.

Urban, J.J. (2017). Emerging scientific and engineering opportunities within the water-energy nexus. Joule *1*, 665–688. https://doi.org/10.1016/j.joule.2017.10.002.

Wang, J.Y., Wang, R.Z., Wang, L.W., and Liu, J.Y. (2017). A high efficient semi-open system for fresh water production from atmosphere. Energy *138*, 542–551. https://doi.org/10.1016/j.energy.2017.07.106.

Wang, W., Xie, S., Pan, Q., Dai, Y., Wang, R., and Ge, T. (2021). Air-cooled adsorption-based device for harvesting water from island air. Renew. Sustain. Energy Rev. *141*, 110802. https://doi.org/10.1016/j.rser.2021.110802.

Watergen. GEN-M world's most efficient water from air generator. https://www.watergen.com/commercial/gen-m/.

Wu, S.L., Chen, H., Wang, H.L., Chen, X., Yang, H.C., and Darling, S.B. (2021). Solar-driven evaporators for water treatment: challenges and opportunities. Environ. Sci. Water Res. Technol. *7*, 24–39. https://doi.org/10.1039/d0ew00725k.

Xu, J., Li, T., Chao, J., Wu, S., Yan, T., Li, W., Cao, B., and Wang, R. (2020). Efficient solar-driven water harvesting from arid air with metal–organic frameworks modified by hygroscopic salt. Angew. Chem. Int. Ed. *59*, 5202–5210. https://doi.org/10.1002/anie.201915170.

Zhao, F., Zhou, X., Liu, Y., Shi, Y., Dai, Y., and Yu, G. (2019). Super moisture-absorbent gels for all-weather atmospheric water harvesting. Adv. Mater. *31*, 1806446. https://doi.org/10.1002/adma.201806446.

Zhou, X., Lu, H., Zhao, F., and Yu, G. (2020a). Atmospheric water harvesting: a review of material and structural designs. ACS Mater. Lett. *2*, 671–684. https://doi.org/10.1021/acsmaterialslett.0c00130.

Zhou, X., Zhang, P., Zhao, F., and Yu, G. (2020b). Super moisture absorbent gels for sustainable agriculture via atmospheric water irrigation. ACS Mater. Lett. *2*, 1419–1422. https://doi.org/10.1021/acsmaterialslett.0c00439.

Zhu, A., Christofides, P.D., and Cohen, Y. (2009). Effect of thermodynamic restriction on energy cost Optimization of RO membrane water desalination. Ind. Eng. Chem. Res. *48*, 6010–6021. https://doi.org/10.1021/ie800735q.

iScience, Volume *24*

Supplemental information

Fresh water production from atmospheric air:

Technology and innovation outlook

Robin Peeters, Hannah Vanderschaeghe, Jan Rongé, and Johan A. Martens

World map of climate conditions

A world map of climate conditions is presented in Figure S1. Ambient relative humidity data is obtained from ERA5 monthly averaged data on pressure levels from 1979 to the present.[1] The pressure level is set to 1000 hPa and monthly averaged data for each hour of a day is used. The 2-meter temperature is obtained from ERA5 monthly averaged data on single levels from 1979 to the present.[2] Both of the datasets are produced by Copernicus Climate Change Service (C3S) which is operated by the European Centre for Medium-Range Weather Forecasts (ECMWF). The monthly averaged data from 2018 to 2020 are loaded in Grid Analysis and Display System (GrADS) to draw the graph. To show the average annual relative humidity at night, information during 21h - 5h local time is averaged and drawn in shaded colors (Figure S1). The final graph combines 24 images of every 15 degrees of longitude to represent each time zone. For instance, 7.5° East to 22.5° East on the graph shows relative humidity information during 21h - 5h of UTC +1. The average annual temperatures are drawn in contour lines. Data of Figure S1 is used to construct Figure 14 in the manuscript. The technology map of Figure 14 is constructed manually at a lower spatial resolution which may result in local deviations of the correct optimal technology choice based on presented climate data.

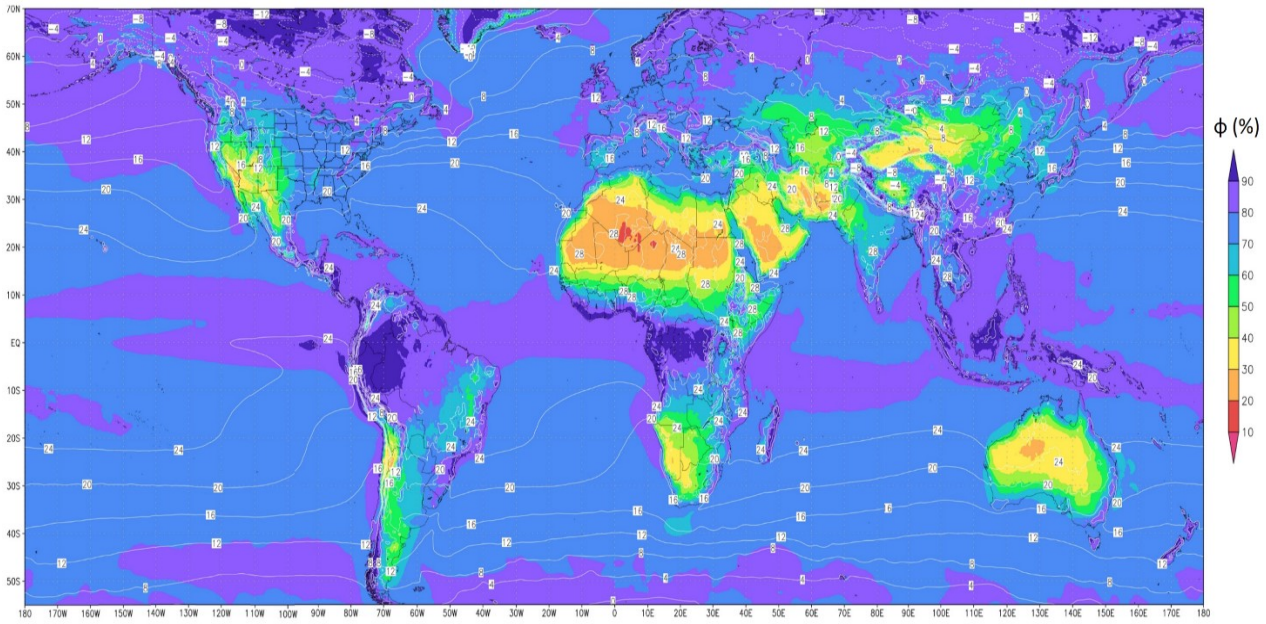

Figure S1. World map of average nightly relative humidity values Φ. Isothermal contour lines indicate average annual temperatures.[1,2] Data of Figure S1 is used to construct Figure 14 in the manuscript.

Supplemental references

1. Hersbach, H., Bell, B., Berrisford, P., Biavati, G., Horányi, A., Muñoz Sabater, J., Nicolas, J., Peubey, C., Radu, R., Rozum, I., et al. (2019). ERA5 monthly averaged data on pressure levels from 1979 to present. Copernicus Climate Change Service (C3S) Climate Data Store (CDS). 10.24381/cds.6860a573.

2. Hersbach, H., Bell, B., Berrisford, P., Biavati, G., Horányi, A., Muñoz Sabater, J., Nicolas, J., Peubey, C., Radu, R., Rozum, I., et al. (2019). ERA5 monthly averaged data on single levels from 1979 to present. Copernicus Climate Change Service (C3S) Climate Data Store (CDS). 10.24381/cds.f17050d7.